Shallow dopant pairs in silicon: An atomistic full configuration interaction study

Archana Tankasala,[1] Benoit Voisin,[2,3] Zachary Kembrey,[2] Joseph Salfi,[4,5] Yu-Ling Hsueh,[2,3] Edyta N. Osika,[2,3] Sven Rogge,[4] and Rajib Rahman[2,3,*]

[1]*Electrical and Computer Engineering, Purdue University, West Lafayette, Indiana 47907, USA*
[2]*School of Physics, The University of New South Wales, Sydney, New South Wales 2052, Australia*
[3]*Silicon Quantum Computing Pty Ltd., Level 2, Newton Building, UNSW Sydney, Kensington, NSW 2052, Australia*
[4]*Centre for Quantum Computation and Communication Technology, School of Physics, The University of New South Wales, Sydney, New South Wales 2052, Australia*
[5]*Department of Electrical Engineering, University of British Columbia, Vancouver, BC V6T 1Z4, Canada*

(Received 10 October 2021; revised 13 April 2022; accepted 13 April 2022; published 29 April 2022)

The two-electron states and exchange couplings are investigated for a phosphorous donor pair in silicon using an atomistic full configuration interaction method for donor separations spanning from 0.4 to 15 nm. Three distinct donor separation regimes appear from our large basis calculations, from which the validity of simplified methods such as Heitler-London and Hartree-Fock type approaches can be assessed. For bulk donors, the exchange coupling saturates below 5 nm due to excited bonding orbital contributions to the wave functions. Ionic contributions to the two-electron state decrease between 5 and 14 nm, and a fully correlated Heitler-London-like state is reached from 14 nm onwards. Oscillations in exchange couplings can be strongly suppressed by placing the donors in the same z plane and at a small depth, D, from the surface. This is a consequence of the z-valley terms becoming dominant within the dopant's wave function and of small changes with x and y separations no longer having much effect. We find the depth to be an important parameter in determining the exchange coupling for subsurface dopants, not only through valley repopulation ($D < 10$ nm) but also through additional interface effects for ultrashallow depths ($D < 2.5$ nm). Our full configuration interaction method provides insights in the exchange interaction for various regimes of donor separation and depths, from the Heitler-London limit at large distances to the 0.4–5 nm range relevant for scanning tunneling microscope based quantum state imaging and spectroscopy experiments. The precise control of electron-electron quantum correlations in such engineered atoms in the solid state is useful to design quantum logic gates and quantum simulators.

DOI: 10.1103/PhysRevB.105.155158

I. INTRODUCTION

Phosphorus donors in silicon have been proposed as the functional block of a silicon quantum information processor that can combine the benefits of single-atom quantum systems with the mature technological platform of silicon [1]. Single-qubit logic has been demonstrated on both electronic and nuclear spins [2,3] bound to these donors along with exceptional coherence times and fidelity [4]. Recently, the first two-qubit logic gate was also demonstrated with dopant atoms coupled by the exchange interaction between electronic spins, thereby providing a proof-of-principle demonstration of universal quantum logic [5]. Coupled dopant atoms are also amenable to quantum simulation of Fermi-Hubbard systems [6,7] and coherent transport of quantum information [8]. The development of atomically precise placement technology for donor atoms in silicon has resulted in a breakthrough in single-atom electronics, with clusters ranging from single to many dopant atoms being realized with deterministic precision [9]. This technology has led to the realization of single-atom transistors [10], atomically thin nanowires [11], single-crystal quantum dots [12,13], and atomically precise tunnel junctions [14], opening up the prospect of a myriad of applications in both classical and quantum electronics.

Direct exchange between electronic spins bound to donors remains the principal method of coupling dopants out of different mechanisms explored both theoretically and experimentally, including long-range dipole-dipole interactions [15,16]. Soon after the original proposal to use the exchange coupling as a means to perform two-qubit logic using dopant atoms [1], it was predicted that the exchange could be highly sensitive to the exact position of the atoms in the lattice due to interference between sixfold degenerate conduction band valley states of silicon [17]. Since then, a body of theoretical works on exchange couplings has appeared in the literature, which mostly focus on the 10- to 20-nm donor separation regime and relies on the effective mass Heitler-London formalism (EMHL) [17–23]. Recent scanning tunneling microscope (STM) based spectroscopy and imaging experiments have also probed directly the nature of the two-electron wave functions of donors separated by a few nanometers and in the proximity of the silicon surface [23]. This closer separation regime offers interesting electronic correlations that can be exploited in quantum simulation [6]. The recently demonstrated two-qubit logic gate [5] also relies on a separation distance of 13 nm, as opposed to the original proposal of a 20-nm separation of Kane [1]. The smaller separations of subsurface

*rajib.rahman@unsw.edu.au

donors of relevance to experiments call for a more detailed investigation of the exchange coupling and electronic correlations of the two-electron donor states beyond the EMHL formalism.

In this work, we investigate the two-electron states of phosphorus donor pairs in silicon using an atomistic full configuration interaction (AFCI) technique. This method provides an exact solution to the two-electron problem for all donor separation regimes within a 20-orbital spin-resolved Slater-Koster tight-binding (TB) method [24]. This approach enables us to assess the regimes of validity of Heitler-London and other simplified many-body approaches for the coupled-donor problem, as well as to track the evolution of electronic correlations as a function of donor separation. Furthermore, the atomistic description of the single-electron states of the donor pairs in TB as a basis for AFCI goes beyond the effective mass approximations, as it includes an atomistic description of interfaces and incorporates conduction band momentum states from a full Brillouin zone (BZ) approach. These considerations are important to reproduce nonbulk experimental situations [23]. The calculations provide us insights into exchange oscillations and how to mitigate these. Lastly, we present calculation results in the regime of 2- to 5-nm separation that was probed in a recent experimental work on STM imaging of exchange-coupled donor pairs [23], showing both exchange and charging energies as a function of depth and separation of the pairs. The atomistic study of the depth dependence of exchange energy down to the sub-Bohr radii distances from the surface is another aspect of this work.

II. METHODOLOGY

The accuracy of an exchange coupling calculation depends on two main factors: (i) the dimensions and the quality of the single-electron basis set, and (ii) the approximations made for the multielectron wave function. In this section, first we compare and contrast between various methodologies with regards to points (i) and (ii) before describing the AFCI methodology in detail.

Even though a hydrogenic donor, such as phosphorus, in silicon has energy states in the band gap within an energy window of about 50 meV below silicon's conduction band minima (CBM), the shallow nature of these states allows the application of the effective mass approximation on the conduction band (CB) with a Coulombic potential well. As a result, envelope functions can be constructed using the transverse and longitudinal effective masses of the CB of silicon. However, the sixfold degeneracy of the CB has to be taken into account in the donor states, and hence, a multivalley Schrödinger equation needs to be solved [20,21,25–35]. A core-correction term, involving a few free parameters, is often introduced to account for the non-Coulombic part of the donor potential close to the nuclear site and to obtain the correct coupling between orbital and valley states (valley-orbit coupling) [25]. Hence, the effective mass solution to the donor wave functions comprises products of hydrogenic envelope functions and Bloch functions of CBM weighted by the valley contributions. In several recent variants of this approach, the Bloch states have been obtained from *ab initio* calculations of a bulk silicon unit cell [36–38]. In realistic donor devices, a nonbulklike scenario often arises from nonuniform local electric fields, interfaces, and strain. To first order, such effects can readjust the weight of the wave function asymmetrically among valley states, an effect known as valley repopulation. Such effects can also change the form of the envelope functions through hybridization with other states in the device.

Beyond effective mass theories, atomistic TB techniques can provide an atomically resolved solution of the donor wave function expanding over several million atoms. The method takes into account realistic interface geometries built from atoms at the surface and uses atomic-orbital-based central-cell corrections for donors which can model different species of donor atoms [39]. Furthermore, TB is a full BZ method and does not assume that CB minima states are the only k states contributing, which are typically important in heterostructures and disordered super lattices. Once the full TB Hamiltonian is set up along with proper device geometry, interface, and applied fields, all the valley-orbital (and spin) states are directly obtained by eigensolving, with no further optimization or parametrization. Other atomistic approaches such as density functional theory are not feasible for exchange calculations due to size limitations, as overlaps between tails of wave functions contribute to exchange energy.

For the two-electron interactions, the full configuration interaction (FCI) method, which solves the two-electron Schrödinger equation in a basis of Slater determinants constructed from the single-electron basis set, is an exact many-body technique that can capture Coulomb, exchange, and higher-order correlations. However, the method is computationally resource consuming, and typically simplified approximations are made. The simplest and most popular method in the literature is the Heitler-London (HL) approximation, which uses a localized orbital for each donor. This method is valid for low wave function overlaps and typically breaks down for close separations and at modest electric fields. In the other scenario, when the two donors are very close, and form strong molecular states, electrons may occupy a superposition of both up- and down-spin configurations of the lowest molecular orbital, a regime that is well-described by the single Slater determinant solution corresponding to a Hartree-Fock (HF)-like approach. A molecular basis configuration interaction was also performed with effective mass wave functions in Ref. [40] but focused on larger donor separations. A recent work has also applied a time-dependent Hartree-Fock approach on this problem with the effective mass wave functions [41]. Our motivation for AFCI therefore stems from the need for accuracy in both the single electron basis and the two-electron methodology.

For the single-electron basis set, we have employed a 20-band spin-resolved $sp^3d^5s^*$ Slater-Koster tight-binding model to obtain the single-electron states of the donor pair [42]. This approach has been well calibrated to experimental measurements of single-donor energy states [39] including the experimentally observed valley-orbital splitting of the $1s$ and higher manifolds [43]. The model has also been validated in a number of joint experiment-theory works on single donors including STM imaging experiments [44] and in calculations of various spin properties, such as hyperfine and spin-orbit Stark effects [45,46], and of spin-lattice relaxation times [47]. The TB Hamiltonian of 1×10^6 to 2×10^6 silicon atoms with

hydrogen-passivated surfaces and two phosphorus atoms with central-cell-corrected Coulomb potential wells are solved using a block Lanczos eigensolver to obtain the molecular states of the dopant pair located just below the bulk conduction band of silicon in energy using NEMO3D [48].

For the two-electron calculations with FCI, a selected set of N low-energy single-electron molecular states are then used to construct all possible Slater determinants (SDs) representing ground and excited configurations of the donor molecule as basis states. The two-electron Hamiltonian $[H(2e)]$ including electron-electron Coulomb interaction is then evaluated between every pair of SDs to obtain a full Hamiltonian of size $C_2^N \times C_2^N$. Here, C_2^N denotes the number of all possible 2-combinations out of the set of N single-electron states. $H(2e)$ is then solved with either LAPACK or FEAST eigensolvers [24] for the total two-electron eigenenergies $[E_{\text{Total}}(2e)]$. The eigenvectors of $H(2e)$ are linear combinations of the SDs, from which spin-singlet and spin-triplet states can be readily identified. The exchange energy ΔE (also labeled as J in this work) is defined as the energy difference between the lowest spin-triplet (E_T) and spin-singlet (E_S) energies, i.e., $\Delta E = E_T - E_S$. This definition of the exchange energy is used all throughout this work irrespective of the orbital symmetries of the states.

We have tested convergence of the FCI results by progressively increasing N and observing whether the two-electron energy changes beyond a numerical tolerance of 10^{-8} eV. For the P-P molecule studied here, we typically found that $N = 24$ was sufficient for convergence for closely separated donors. For far-separated donors, even $N = 4$ can provide converged solutions, consistent with the Heitler-London wave functions analyzed later. The single-electron TB solutions typically take 3–4 h on 48 processors, while the two-electron AFCI calculations with $N = 24$ takes 2 h on 300 processors. The most time-consuming part is evaluating the Coulomb and exchange integrals between sets of four wave functions each of which spans over 1×10^6 to 2×10^6 atoms and 20 orbitals per atom.

Further implementation details of the AFCI method can be found in Ref. [24], where the technique was applied to solve the challenging problem of two electrons bound (D^-) to a single phosphorus donor in silicon. Excellent quantitative agreement was obtained with experimentally measured binding and charging energies both for a bulk donor and for donors closer to an interface and subject to an electric field [49]. The D^- problem is a difficult calculation with FCI because many single-electron states, even from the higher $2s$, $3s$, and $4s$ manifolds, are needed to build up the expanded valley-orbital states of the two electrons. Additionally, in Ref. [50], we have extensively applied the AFCI technique on two electrons bound to a cluster of well-separated donors and showed how the voltage dependency of the exchange coupling can be increased by several orders of magnitude. These give us confidence that the AFCI method captures both the single-particle physics and the two-electron correlations accurately.

III. RESULTS AND ANALYSIS

Figures 1(a) and 1(b) show schematics of the silicon crystal we investigate. They also define all the geometric parameters of interest such as the donor separation R, the donor depth

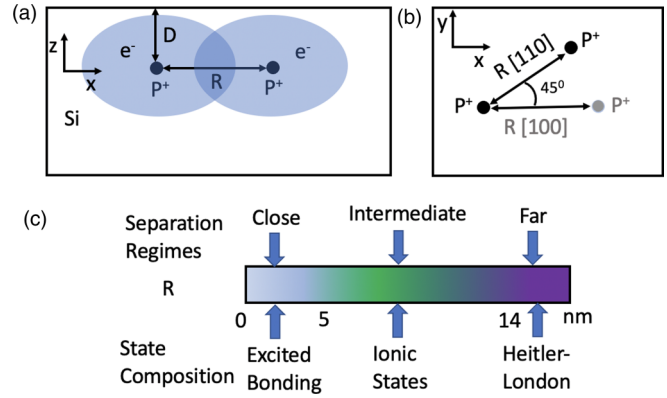

FIG. 1. (a) Schematic of two phosphorus impurity ions (P^+) with two bound electrons embedded in a silicon crystal. The P atoms are separated by a distance R and are placed at a depth D from the surface in the z direction. (b) Schematic of an xy plane of the silicon lattice showing two distinct separation axes of the donors, [110] and [100]. (c) Breakdown of the analysis of the calculations into three regimes of separation, far (14 nm and larger), intermediate (5–14 nm), and close (0.4–5 nm) spacings. As we show later, the nature of the two-electron wave functions differ in these regimes and can be linked with well-known approximations, such as Heitler-London and Hund Mulliken (ionic), for certain separations.

D below the surface in z, and the separation axes [100] and [110]. Based on FCI calculations shown later, we can identify three donor separation regimes as shown in Fig. 1(c). In the close-separation regime ($R < 5$ nm) of relevance to STM imaging experiments, the P-P molecule is in the strongly coupled regime where the electrons are fully delocalized between the two P atoms and are strongly affected by Coulomb interactions and screening. In the far-separated regime ($R > 14$ nm), of relevance to qubits, the electrons are weakly coupled and are highly localized. The intermediate-separation regime (5–14 nm), also of relevance to qubits and quantum simulations, shows a gradual transition between the close-separation and the far-separation regimes.

A. Exchange saturation at small donor separations

The exchange (J) evaluated for large donor separations using the HL method is known to increase exponentially with decreasing donor separations, albeit oscillations in certain directions [17]. AFCI allows us to explore if this trend also holds for closer donor separations, where the HL method is not expected to be valid. Figure 2(a) shows the exchange energy as a function of donor separation from 0.38 to 15 nm along [110] for donors at three different depths, $3.5a_0$, $6.25a_0$, and $28.5a_0$ (or bulklike), where $a_0 = 0.543\,095$ nm is the silicon crystal lattice constant. We chose the [110] direction as exchange oscillations are clearly visible for relative donor positions changing by $\frac{1}{\sqrt{2}}\,a_0$ (0.38 nm) in that direction. From the log-linear scale of Fig. 2(a), we see the exponential increase and J oscillations down to donor separations of 5 nm, corroborating the HL trends from literature. However, we find that the exchange energy saturates for donors closer than a critical separation distance of 5 nm.

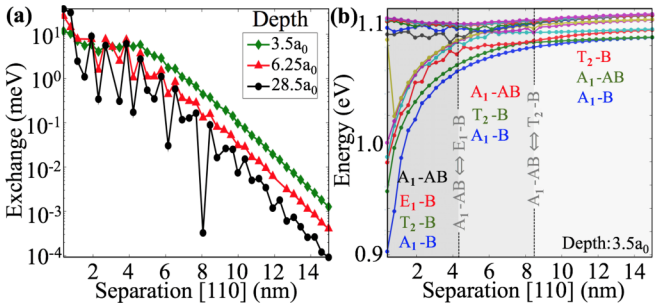

FIG. 2. (a) Exchange energy of donor pairs obtained from atomistic configuration interaction calculations as a function of donor separation along the [110] crystallographic axis, for three different donor depths from the surface. The depth $28.5a_0$ represents a bulklike donor, reproduced here from Ref. [50]. The exchange energy saturates for donor separations below 5 nm, and the oscillations in exchange are strongly suppressed for shallow depths. (b) Single-electron energy levels of the donor pairs located at $3.5a_0$ from the silicon surface relative to the bulk valence band maxima of silicon in the tight-binding model (at 0 eV). The conduction band minima is at 1.131 355 eV. The A_1, T_2 and E_1 states follow labels from group theory (based on symmetry) for the six $1s$-like states of a single donor in bulk silicon [25]. In a coupled donor molecule, pairs of states can form bonding (B) or antibonding (AB) states. While the B and AB states come in pairs for far-separated donors, closer separations lower the B states in energy due to larger B-AB splittings.

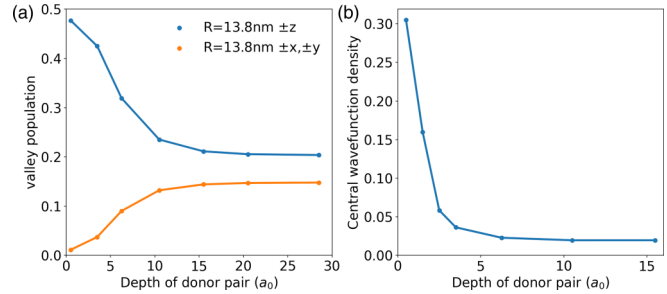

FIG. 3. (a) Valley population of the lowest bonding state as a function of the depth of the donor pair separated by $R = 13.8$ nm along [110]. The z valleys dominate at shallow depth and saturate to a moderate value when the depth of the donors is large enough to be considered bulk. The valley populations are calculated from the valley peak heights of the Fourier transform of the single-electron (bonding) ground state obtained in real space. (b) Central wavefunction density between the donors as a function of donor depth for the same donor pair as in panel (a). This is calculated by summing the square amplitude of the wave function between the two planes perpendicular to the donor axis from 1/4 to 3/4 of the separation R.

To understand these observed trends, we show the single-electron energy levels of the two donors at a shallow depth in Fig. 2(b). In a bulk donor, the six $1s$ states are split into states of A_1 (1), T_2 (3), and E_1 (2) symmetry, with energies of 45.6, 33.9, and 32.6 meV below the CB minima, respectively, where the numbers included in parentheses indicate their degeneracy excluding spin [25,29]. Each of these states in a donor pair can form both bonding (B) and antibonding (AB) states through tunnel coupling. In the large-separation regime, the splitting between these B and AB states is small, hence the A_1-B and A_1-AB states remain far separated from the T_2 and E_1 manifolds due to the large energy gap between the A_1 and these excited manifolds. However, as the donor separation decreases, the B-AB splitting increases, and ultimately the A_1-AB state anticrosses the T_2-B state, as shown in Fig. 2(b). As the donor separation decreases, the B-AB splitting increases among all the valley-orbital states, and below 5 nm, the lowest six states are all bonding states. This changes the symmetry of the donor molecule since the two electrons now occupy the bonding states instead of A_1-B and A_1-AB states. Further decreasing the donor separation does not affect the splitting between the A_1 and T_2 bonding states as much as that of the A_1-B and A_1-AB states since the splitting between the A_1 and T_2 bonding states mostly depends on the valley-orbit interaction. Thus, the exchange saturates once the two-electron states mainly consist of the bonding states.

B. Suppressed exchange oscillations for subsurface donors

The AFCI results in Fig. 2(a) show the variation in exchange with donor separations along [110] diminishes as the depth reduces from $28.5a_0$ (bulk) to $6.25a_0$ and ultimately gets completely suppressed at $3.5a_0$. It is also observed that for donor separations larger than 5 nm the magnitude of J increases with decreasing depth, while a monotonic increase in J cannot be observed for all the data points for $R < 5$ nm. However, the J oscillations with in-plane donor locations still diminish for all donor separations as depth is decreased.

Both suppression of exchange variation and increase in its amplitude can be explained to first order by an increase of the confinement along the direction perpendicular to the interface, z in this case. For donors separated in the xy plane, the exchange oscillations arise from valley interference of the x and y valleys. At $28.5a_0$ depth mimicking a bulklike scenario, the x, y, and z valleys are all contributing similarly to the donor wave function, with the z-valley weight slightly dominating over the x and y (shown later) due to the confinement asymmetry of the potential. When the three valley weights are similar, a small change in the in-plane separation of the donor affects both the x- and the y-valley interference and, thus, the exchange J. At smaller donor depths, the stronger interface confinement increases the energies of the x and y valleys more than the z valleys since the x and y valleys have smaller effective mass along the z direction. Therefore, the lower energy states of the subsurface donors are z-valley dominant, as shown in Fig. 3(a) where the valley population was obtained through the Fourier transform of the real-space wave function. The x- and y-valley populations are much smaller, and therefore, the xy-valley interference has a much smaller effect on J. This valley repopulation also means that the anisotropic effective mass of the valleys plays a more prominent role in the xy confinement of the wave function. When the wave function is equally distributed over all six valleys, the wave-function confinement is determined by the heavier longitudinal mass of each valley, which yields an equal wave-function extent in each direction. However, for the dominant z-valley contribution, the xy wave-function extent is dictated by the lighter transverse effective mass of the z valleys. As a result, the overlap between the two donor

wave functions increases in the xy direction and causes an increase in J. This is highlighted in Fig. 3(b), which shows the integrated electron density over a region centered in between the two donors, indicative of the wave-function overlap in the molecular orbital basis.

Suppressed exchange oscillations closer to the surface may minimize statistical fluctuations of J from qubit to qubit, particularly when the STM lithography can place the donors in-plane and minimize straggle in z [22]. Note that J oscillations are still expected for depth variations through the dominant z-valley contributions.

For donor separations smaller than 5 nm, the value of J does not always increase as the depth decreases, even though the J oscillations with R are suppressed at smaller depths. In this small-separation regime, there is J saturation arising from the excited bonding orbitals that contribute to the two-electron ground state significantly (shown later). Since these bonding orbitals from the T_2 and E manifolds still have significant xy-valley population, we do not see the exchange splitting monotonically increasing due to the single (z)-valley effective mass anisotropy. There are additional effects beyond valley repopulation that emerge when the interface is within 2 Bohr radii of the wave function, as discussed later. Unlike most other approximate calculation methods, this regime of small R and small D can be captured by AFCI.

C. Angular dependence of exchange and charging energy

In this section, we perform FCI calculations of exchange and charging energies in donor pairs as a function of in-plane angular separations from [100] to [110]. We focus on a separation regime of 2–5 nm and a typical depth of $4.5a_0$ for both donors. These donor configurations are of relevance to STM imaging and spectroscopy experiments [23], which aim to resolve wave-function interference and to establish its links with J coupling. This is a regime where the distinct identities of the two donors are still preserved, while electron-electron interactions and J couplings are large enough to be probed. These theoretical calculations further substantiate the experimental results [23].

The two-electron charging energy (CE) is the energy required to overcome the electron-electron interaction to load the second electron to the donor pair. Experimentally, this can be directly measured from the charge stability diagram (conductance vs gate bias) using electrostatic lever arms or capacitances of the gates. The CE is dominated by the Coulomb repulsion energy of the electrons. Hence, the measurement of the CE can also be used to identify the number of bound electrons to the donor pair [13]. For example, the CE of the third electron is expected to be much less than that of the second electron, as the wave functions spread out more with higher number of electrons and the corresponding Coulomb repulsion reduces. Hence, it is important to know the range of possible CEs with donor separations. This may also help to obtain information about donor separations in experiments directly from transport measurements. The CE is the total energy difference between the interacting and the noninteracting two-electron systems,

$$\mathrm{CE} = E_{\text{Total-GS}}(2e) - 2 * E_{\text{Total-GS}}(1e), \tag{1}$$

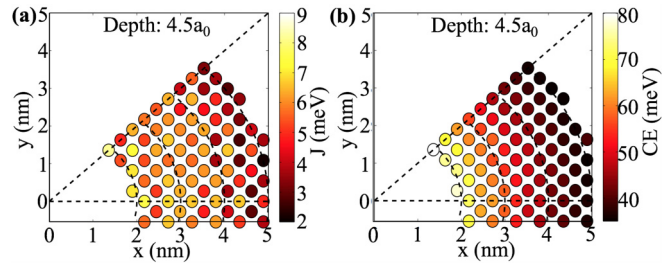

FIG. 4. Exchange energy J and $1e^- \rightarrow 2e^-$ charging energy (CE) of shallow donor pairs. (a) J is shown (in color) at varying donor separations in the xy plane (from 2 to 5 nm) and separation directions (from [100] to [110]). The exchange J varies by less than an order of magnitude for shallow donors due to z-valley repopulation. (b) CE (in color) for the same distance range is more monotonic compared to J.

where $E_{\text{Total-GS}}(2e)$ is the total energy of the two-electron ground state, and $E_{\text{Total-GS}}(1e)$ is the single-electron ground-state orbital energy. Similarly, the binding energy (BE) of the second electron relative to the conduction band minima ($\mathrm{CB_{min}}$) is given by

$$\mathrm{BE} = E_{\text{Total-GS}}(2e) - \mathrm{CB_{min}} - E_{\text{Total-GS}}(1e). \tag{2}$$

Hence,

$$\mathrm{BE} = \mathrm{CE} + E_{\text{Total-GS}}(1e) - \mathrm{CB_{min}}. \tag{3}$$

For a bound orbital, $E_{\text{Total-GS}}(1e) - \mathrm{CB_{min}}$ is negative. The CE, for repulsive electron-electron interaction is, on the other hand, positive. For the second electron to be bound, BE has to be negative. Hence, $|\mathrm{CE}| < |E_{\text{Total-GS}}(1e) - \mathrm{CB_{min}}|$ for a two-electron bound state. This means that the electron-electron interaction obstructs the loading of the second electron, and the second electron can be bound to the two-phosphorus molecule if CE does not overcome the negative single-electron orbital energy.

Figures 4(a) and 4(b) show the exchange and charging energies, respectively, for all possible in-plane lattice positions when one donor is located at the origin and the other donor at the circled positions 2–5 nm away. The color scale indicates the magnitudes of J and CE. The exchange oscillations are smaller by about an order of magnitude for this shallow depth compared to bulk, irrespective of the donor separation direction. The two-electron CE, which is dominated by the Coulomb repulsion energy, does not oscillate like J. In fact, the CE changes rather monotonically with the donor separations and remains nearly constant with the donor separation direction, as seen from Fig. 4(b).

D. Oscillations in exchange with depth variation

Figure 5(a) shows the exchange energy variations with the depth D of coplanar donors, for a fixed separation R of 3 nm along [100]. The depth variation here is within several Bohr radii of the donor wave function. While valley repopulation effects are still present, there are excited bonding orbitals at play in this regime of J saturation. Furthermore, these excited states do not have the well-defined valley-orbital ($1s - T_2$- and $1s - E_1$-like) symmetry of bulk states, as the interface

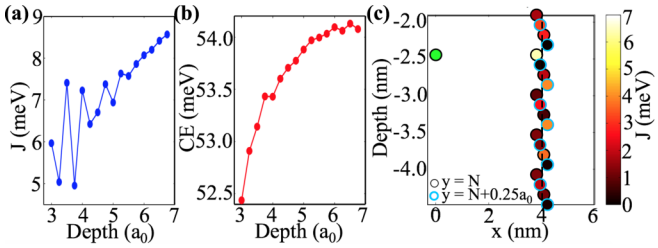

FIG. 5. Effect of donor depth on J and CE. (a) J for donors separated by 3 nm along [100] with increasing donor depths. (b) CE for the same donor locations as in panel (a) is again more monotonic and saturates to its corresponding bulk value. (c) J for donor pairs where one donor is fixed (green dot) at $4.5a_0$ from the silicon surface, with varying depth of the second donor. Lattice points circled in black and blue correspond to slightly different y positions that alternate between adjacent monolayers by $0.25a_0$.

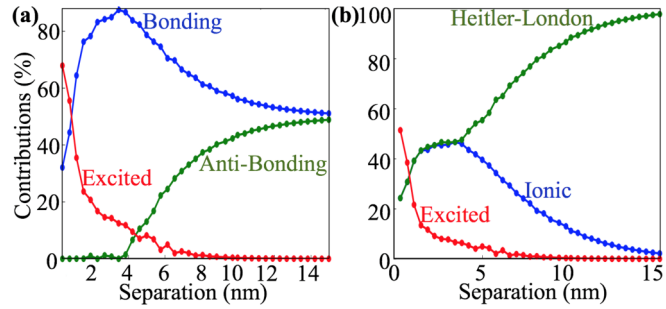

FIG. 6. Assessment of approximate methods for calculating the two-electron ground state of a donor pair from AFCI. The donors are located $4.5a_0$ below the silicon surface, separated along [110]. (a) Contributions of bonding states, antibonding states, and all the remaining (excited) states to the ground state. For donor separations larger than 14 nm (the Heitler-London regime) the bonding and antibonding contributions are equal and there are no contributions from any other (excited) states of the donors. (b) Contributions from the Heitler-London wave function, the ionic (two-electron on the same site) wave function, and all the remaining (excited) wave functions. For separations below 5 nm, there is a significant contribution from the excited states of the donor that is not captured in a Hartree-Fock-like single Slater determinant approximation.

significantly modifies both their valley and their orbital components. Hence, the trends in J with depth does not follow the same monotonic behavior as in the case of large R. The reasoning based on the single z-valley effective mass anisotropy is no longer applicable here, as there are still non-negligible x and y valleys through the excited bonding states. In the particular case of R and D shown here, we find that as the depth decreases, J decreases, which is an opposite trend to the HL regime. Also, we observe that J oscillates with D at about 2 Bohr radii depth. Such oscillations can emerge from the sharp confining potential of the interface, which introduces an additional source of interference through the z-valley phase in the wave function.

The CE for this donor pair shows a limited increase with depths of less than 2 meV [Fig. 5(b)]. The CE saturates to the bulk values as the depth of the donor pair increases, and more Coulomb-like symmetry is restored.

We also investigated the impact of a relative depth between the two donors, which modifies the z-valley interference condition. When there is a difference in the relative depths of the two donors, the z-valley interference is affected by this difference. Due to high z-valley population in subsurface donors, a small change in relative donor depths can lead to a significant change in J. Figure 5(c) shows exchange energy (in color) as a function of depth of one donor with the other donor fixed at $4.5a_0$ from the silicon surface. The exchange energy in this case is sensitive to the relative depth due to the z-valley interference, highlighting the relevance of keeping the donors in the same plane during fabrication.

E. Regimes of validity of approximate calculation methods for exchange energy

The AFCI method helps to evaluate the contributions of various molecular orbital states to the two-electron ground state as a function of donor separation. This is shown in Fig. 6(a) for a donor pair at $4.5a_0$ depth and separated along [110]. The eigenvectors solved from AFCI are normalized linear combinations of two-electron SDs composed of spin-resolved molecular orbitals of the system. Hence, from the coefficients of these SDs, we can obtain the percentage contributions. It is observed that the lowest (A_1) bonding and antibonding orbitals have almost equal (50% each) contributions for large donor separations of about 14 nm and more. Hence, this large-separation regime is given by a linear combination of two SDs, reminiscent of a HL regime. As the donor separation decreases, the contribution of the bonding SD increases and that of the antibonding SD decreases. Between 3 and 5 nm, we observe the bonding SD contribution is so dominant (above 80%) that the ground state can almost be approximated with a single SD comprising the bonding orbital with up and down spins. This is, therefore, more in the regime of a HF-like solution, where a single SD is a good approximation to the many-body ground state. However, AFCI also shows that this approximation is also not fully correct for the donor-pair problem, as excited orbitals from other valley symmetries (T_2, E) begin to contribute to the ground state. At donor separations smaller than 4 nm, we observe that the excited SD contributions grow considerably (while the antibonding SD contributions drop to zero). At about $R = 2$ nm, these excited SD contributions even exceed those of the A_1 bonding SD. This causes a change in the valley-orbit symmetry of the donor molecule at very small separations.

Electron interactions are often evaluated in literature using approximate methods such as HL or HF type approaches. AFCI helps to assess the validity of these approximations as a function of donor separations. This is shown in Fig. 6(b). The HL approximation assumes that the electrons are localized in different donors, and uses a two-electron wave function of the form

$$\psi(r_1, r_2) = \tfrac{1}{2}[\phi_L(r_1)\phi_R(r_2) + \phi_R(r_1)\phi_L(r_2)] \times (\uparrow_1\downarrow_2 - \downarrow_1\uparrow_2), \quad (4)$$

where ϕ_L and ϕ_R are orbitals localized to the left and right donors, respectively. Here, the spatial coordinates of the

electrons are represented as r_1 and r_2, and their spins are $\downarrow$ and $\uparrow$ with subscripts 1 and 2. The orbital part of this state is symmetric and the spin part is antisymmetric, making the total wave function antisymmetric. In an orthogonal molecular orbital basis, this same state is given as a linear combination of two SDs of the form

$$\psi(r_1, r_2) = \frac{1}{\sqrt{2}}[\phi_B(r_1)\phi_B(r_2)](\uparrow_1\downarrow_2 - \downarrow_1\uparrow_2) + \frac{1}{\sqrt{2}}[\phi_{AB}(r_1)\phi_{AB}(r_2)](\uparrow_1\downarrow_2 - \downarrow_1\uparrow_2), \quad (5)$$

where ϕ_B and ϕ_{AB} are the bonding and the antibonding orbitals. By making the substitutions $\phi_B = \frac{1}{\sqrt{2}}(\phi_L + \phi_R)$ and $\phi_{AB} = \frac{1}{\sqrt{2}}(\phi_L - \phi_R)$, Eq. (5) reduces to the HL form of Eq. (4).

The HL wave function, however, ignores ionic contributions in which both electrons are located either on the left donor or on the right donor. These ionic contributions are stronger for smaller separations of donor pairs and are given by a Hartree-Fock type wave function, such as

$$\psi(r_1, r_2) = \frac{1}{2\sqrt{2}}[\phi_L(r_1)\phi_L(r_2) + \phi_L(r_1)\phi_R(r_2) + \phi_R(r_1)\phi_L(r_2) + \phi_R(r_1)\phi_R(r_2)] \times (\uparrow_1\downarrow_2 - \downarrow_1\uparrow_2). \quad (6)$$

The single SD with bonding orbitals yields a wave function of this form,

$$\psi(r_1, r_2) = \frac{1}{\sqrt{2}}[\phi_B(r_1)\phi_B(r_2)](\uparrow_1\downarrow_2 - \downarrow_1\uparrow_2). \quad (7)$$

Again, Eq. (7) reduces to Eq. (6) when we make the substitution $\phi_B = \frac{1}{\sqrt{2}}(\phi_L + \phi_R)$. In other words, we obtain the single SD Hartree-Fock type solution when the antibonding SD contribution diminishes from the HL wave function.

Figure 6(b) decomposes the FCI wave function solution as comprising HL, ionic (HF), or excited two-electron configurations. For donors separated by 14 nm and above, a true HL state is formed with two SDs in the molecular orbital (MO) basis. This correlated regime cannot be expressed by a single SD in the MO basis. As the donor separation decreases, the ionic contributions build up while the HL contributions diminish in the FCI wave function. This amounts to a cancellation of the antibonding SDs from the HL wave function by the ionic contributions, and between 3 and 5 nm, we witness an uncorrelated, Hartree-Fock-like regime. However, FCI also shows, as discussed earlier, significant contributions from excited SDs from other valley-orbit symmetries contributing to the wave function for very close donor separations.

We have restricted our analysis in this section to the singlet state only, as it is trivial to do the same analysis on the triplet state. The essential difference between the two states are the sign changes to interchange the symmetric and antisymmetric parts of the wave function. For the triplet state, the orbital part of the wave function is antisymmetric and the spin part is symmetric, which preserves the antisymmetry of the entire wave function over both spin and charge.

IV. CONCLUSION

We have developed a computational framework to calculate exchange and charging energies using a full configuration interaction method which solves an interacting $2e$ Hamiltonian using an atomistic tight-binding based single-electron basis. Using this approach, the validity of approximate methods can be assessed as a function of the separation between the donors. The Heitler-London state becomes fully valid for donor separations beyond 14 nm. A single Slater determinant solution in the molecular orbital basis in the spirit of Hartree-Fock gives a good representation of the wave function for a range between 3 and 5 nm of interest in STM imaging and spectroscopy experiments. However, AFCI calculations reveal the growing influence of excited states in the wave functions in the small-separation regime of 3 nm and below. Approximate methods for J calculations do not typically account for these states. In this close distance regime, the influence of higher bonding orbitals causes the exchange to saturate. The oscillations in exchange with donor separation along [110] are also shown to be suppressed for shallow donors

TABLE I. Summary of R and D dependence of J. The symbol WF denotes wave functions, HL denotes Heitler-London, and HF denotes Hartree-Fock.

D \ R	Small (0.4–5 nm)	Intermediate–large (>5 nm)
Small (<5 nm)	J: Oscillating with D, suppressed oscillations with R, saturation in average magnitude with R WF: Excited orbital contributions Valleys: Case-by-case analysis needed based on R and D	J: Larger magnitude compared to large D, strongly suppressed oscillations with R, exponential drop with R WF: HL at large R to ionic (HF-like) at intermediate R, large overlap due to small D Valleys: z-valley dominant
Large (>5 nm)	J: Pronounced oscillations with R, saturation in average magnitude with R WF: Large contribution from excited bonding orbitals Valleys: z-valley dominant in ground orbital, x and y valleys from excited orbitals	J: Noticeable oscillations with R, exponential drop with R WF: HL at large R to ionic (HF-like) at intermediate R, small WF overlap due to large D Valleys: Slight asymmetry in valley populations due to separation axis

located close to the interface. This is due to an increase in the z-valley population that makes exchange more immune to donor separation along the x and y directions, but the exchange oscillations remain present with varying donor depths due to the associated changes in the z-valley interference condition. Relative donor depths and close proximity of interfaces are also seen to induce oscillations in exchange coupling, which emphasizes the need to precisely control the vertical straggle in donor positions. Table I summarizes the main features of the two-electron states as observed from the FCI simulations.

Although the methodology developed here is applied to phosphorus donors, the same technique can be applied to other shallow donor and acceptor pairs (groups III and VI) in silicon and germanium. The main difference will arise from the single-electron wave functions of the dopants. For example, the deeper the binding energy of the dopant, the stronger the electron density in the central cell, which means that the tail of the wave function will reduce in its extent. This will also reduce the exchange splitting, but one can still observe the various regimes of exchange energy. They will only occur at slightly reduced separations. For very deep donors, the tight-binding method may no longer be applicable due to the subatomically confined wave functions and more complicated electron-electron interactions in the core of the impurity species. For shallow acceptor pairs, such as boron [51], exchange oscillations are not expected as the valence-band maxima states occur at $k = 0$. The method is also applicable directly to such dopants embedded in realistic devices, which may have applied gate voltages or strain, and requires no additional computational costs.

ACKNOWLEDGMENTS

This work is funded by the ARC Center of Excellence for Quantum Computation and Communication Technology (Grant No. CE170100012), an ARC Discovery Project (Grant No. DP180102620), and in part by the U.S. Army Research Office (Grant No. W911NF-17-1-0202). Computational resources from NCN/NanoHub.org and the Rosen Center for Advanced Computing (RCAC) at Purdue are acknowledged. We also acknowledge computational resources and services from the National Computational Infrastructure (NCI) under NCMAS 2020 and 2021 allocations, supported by the Australian Government, and from the computational cluster Katana supported by Research Technology Services at UNSW Sydney.

[1] B. E. Kane, A silicon-based nuclear spin quantum computer, Nature (London) **393**, 133 (1998).

[2] J. J. Pla, K. Y. Tan, J. P. Dehollain, W. H. Lim, J. J. L. Morton, D. N. Jamieson, A. S. Dzurak, and A. Morello, A single-atom electron spin qubit in silicon, Nature (London) **489**, 541 (2012).

[3] J. J. Pla, K. Y. Tan, J. P. Dehollain, W. H. Lim, J. J. L. Morton, F. A. Zwanenburg, D. N. Jamieson, A. S. Dzurak, and A. Morello, High-fidelity readout and control of a nuclear spin qubit in silicon, Nature (London) **496**, 334 (2013).

[4] J. T. Muhonen, J. P. Dehollain, A. Laucht, F. E. Hudson, R. Kalra, T. Sekiguchi, K. M. Itoh, D. N. Jamieson, J. C. McCallum, A. S. Dzurak, and A. Morello, Storing quantum information for 30 seconds in a nanoelectronic device, Nat. Nanotechnol. **9**, 986 (2014).

[5] Y. He, S. K. Gorman, D. Keith, L. Kranz, J. G. Keizer, and M. Y. Simmons, A two-qubit gate between phosphorus donor electrons in silicon, Nature (London) **571**, 371 (2019).

[6] J. Salfi, J. A. Mol, R. Rahman, G. Klimeck, M. Y. Simmons, L. C. L. Hollenberg, and S. Rogge, Quantum simulation of the Hubbard model with dopant atoms in silicon, Nat. Commun. **7**, 11342 (2016).

[7] N. H. Le, A. J. Fisher, N. J. Curson, and E. Ginossar, Topological phases of a dimerized Fermi–Hubbard model for semiconductor nano-lattices, npj Quantum Inf. **6**, 24 (2020).

[8] F. A. Mohiyaddin, R. Kalra, A. Laucht, R. Rahman, G. Klimeck, and A. Morello, Transport of spin qubits with donor chains under realistic experimental conditions, Phys. Rev. B **94**, 045314 (2016).

[9] S. R. Schofield, N. J. Curson, M. Y. Simmons, F. J. Rueß, T. Hallam, L. Oberbeck, and R. G. Clark, Atomically Precise Placement of Single Dopants in Si, Phys. Rev. Lett. **91**, 136104 (2003).

[10] M. Fuechsle, J. A. Miwa, S. Mahapatra, H. Ryu, S. Lee, O. Warschkow, L. C. L. Hollenberg, G. Klimeck, and M. Y. Simmons, A single-atom transistor, Nat. Nanotechnol. **7**, 242 (2012).

[11] B. Weber, S. Mahapatra, H. Ryu, S. Lee, A. Fuhrer, T. C. G. Reusch, D. L. Thompson, W. C. T. Lee, G. Klimeck, L. C. L. Hollenberg, and M. Y. Simmons, Ohm's Law survives to the atomic scale, Science **335**, 64 (2012).

[12] M. Fuechsle, S. Mahapatra, F. A. Zwanenburg, M. Friesen, M. A. Eriksson, and M. Y. Simmons, Spectroscopy of few-electron single-crystal silicon quantum dots, Nat. Nanotechnol. **5**, 502 (2010).

[13] B. Weber, Y. H. M. Tan, S. Mahapatra, T. F. Watson, H. Ryu, R. Rahman, L. C. L. Hollenberg, G. Klimeck, and M. Y. Simmons, Spin blockade and exchange in Coulomb-confined silicon double quantum dots, Nat. Nanotechnol. **9**, 430 (2014).

[14] X. Wang, J. Wyrick, R. V. Kashid, P. Namboodiri, S. W. Schmucker, A. Murphy, M. D. Stewart, and R. M. Silver, Atomic-scale control of tunneling in donor-based devices, Commun. Phys. **3**, 82 (2020).

[15] G. Tosi, F. A. Mohiyaddin, V. Schmitt, S. Tenberg, R. Rahman, G. Klimeck, and A. Morello, Silicon quantum processor with robust long-distance qubit couplings, Nat. Commun. **8**, 450 (2017).

[16] C. D. Hill, E. Peretz, S. J. Hile, M. G. House, M. Fuechsle, S. Rogge, M. Y. Simmons, and L. C. L. Hollenberg, A surface code quantum computer in silicon, Sci. Adv. **1**, e1500707 (2015).

[17] B. Koiller, X. Hu, and S. Das Sarma, Exchange in Silicon-Based Quantum Computer Architecture, Phys. Rev. Lett. **88**, 027903 (2001).

[18] C. J. Wellard, L. C. L. Hollenberg, F. Parisoli, L. M. Kettle, H.-S. Goan, J. A. L. McIntosh, and D. N. Jamieson, Electron

exchange coupling for single-donor solid-state spin qubits, Phys. Rev. B **68**, 195209 (2003).

[19] L. M. Kettle, H.-S. Goan, S. C. Smith, L. C. L. Hollenberg, and C. J. Wellard, The effects of J-gate potential and interfaces on donor exchange coupling in the Kane quantum computer architecture, J. Phys.: Condens. Matter **16**, 1011 (2004).

[20] G. Pica, B. W. Lovett, R. N. Bhatt, and S. A. Lyon, Exchange coupling between silicon donors: The crucial role of the central cell and mass anisotropy, Phys. Rev. B **89**, 235306 (2014).

[21] A. L. Saraiva, A. Baena, M. J. Calderón, and B. Koiller, Theory of one and two donors in silicon, J. Phys.: Condens. Matter **27**, 154208 (2015).

[22] Y. Song and S. Das Sarma, Statistical exchange-coupling errors and the practicality of scalable silicon donor qubits, Appl. Phys. Lett. **109**, 253113 (2016).

[23] B. Voisin, J. Bocquel, A. Tankasala, M. Usman, J. Salfi, R. Rahman, M. Y. Simmons, L. C. L. Hollenberg, and S. Rogge, Valley interference and spin exchange at the atomic scale in silicon, Nat. Commun. **11**, 6124 (2020).

[24] A. Tankasala, J. Salfi, J. Bocquel, B. Voisin, M. Usman, G. Klimeck, M. Y. Simmons, L. C. L. Hollenberg, S. Rogge, and R. Rahman, Two-electron states of a group-V donor in silicon from atomistic full configuration interactions, Phys. Rev. B **97**, 195301 (2018).

[25] W. Kohn and J. M. Luttinger, Theory of donor states in silicon, Phys. Rev. **98**, 915 (1955).

[26] H. Fritzsche, Effect of stress on the donor wave functions in germanium, Phys. Rev. **125**, 1560 (1962).

[27] S. T. Pantelides and C. T. Sah, Theory of localized states in semiconductors. I. New results using an old method, Phys. Rev. B **10**, 621 (1974).

[28] T. H. Ning and C. T. Sah, Multivalley effective-mass approximation for donor states in silicon. I. Shallow-level group-V impurities, Phys. Rev. B **4**, 3468 (1971).

[29] A. K. Ramdas and S. Rodriguez, Spectroscopy of the solid-state analogues of the hydrogen atom: Donors and acceptors in semiconductors, Rep. Prog. Phys. **44**, 1297 (1981).

[30] L. M. Kettle, H.-S. Goan, S. C. Smith, C. J. Wellard, L. C. L. Hollenberg, and C. I. Pakes, Numerical study of hydrogenic effective mass theory for an impurity P donor in Si in the presence of an electric field and interfaces, Phys. Rev. B **68**, 075317 (2003).

[31] M. Friesen, Theory of the Stark Effect for P Donors in Si, Phys. Rev. Lett. **94**, 186403 (2005).

[32] G. D. J. Smit, S. Rogge, J. Caro, and T. M. Klapwijk, Stark effect in shallow impurities in Si, Phys. Rev. B **70**, 035206 (2004).

[33] A. Debernardi, A. Baldereschi, and M. Fanciulli, Computation of the Stark effect in P impurity states in silicon, Phys. Rev. B **74**, 035202 (2006).

[34] M. J. Calderón, A. Saraiva, B. Koiller, and S. Das Sarma, Quantum control and manipulation of donor electrons in Si-based quantum computing, J. Appl. Phys. **105**, 122410 (2009).

[35] M. V. Klymenko, S. Rogge, and F. Remacle, Multivalley envelope function equations and effective potentials for phosphorus impurity in silicon, Phys. Rev. B **92**, 195302 (2015).

[36] B. Koiller, R. B. Capaz, X. Hu, and S. Das Sarma, Shallow-donor wave functions and donor-pair exchange in silicon: *Ab initio* theory and floating-phase Heitler-London approach, Phys. Rev. B **70**, 115207 (2004).

[37] C. J. Wellard and L. C. L. Hollenberg, Donor electron wave functions for phosphorus in silicon: Beyond effective-mass theory, Phys. Rev. B **72**, 085202 (2005).

[38] J. K. Gamble, N. T. Jacobson, E. Nielsen, A. D. Baczewski, J. E. Moussa, I. Montaño, and R. P. Muller, Multivalley effective mass theory simulation of donors in silicon, Phys. Rev. B **91**, 235318 (2015).

[39] S. Ahmed, N. Kharche, R. Rahman, M. Usman, S. Lee, H. Ryu, H. Bae, S. Clark, B. Haley, M. Naumov *et al.*, Multimillion Atom Simulations with Nemo3D, in *Encyclopedia of Complexity and Systems Science* (Springer, Berlin, 2009), pp. 5745–5783.

[40] L. M. Kettle, H.-S. Goan, and S. C. Smith, Molecular orbital calculations of two-electron states for P-donor solid-state spin qubits, Phys. Rev. B **73**, 115205 (2006).

[41] W. Wu and A. J. Fisher, Excited states of a phosphorus pair in silicon: Combining valley-orbital interaction and electron-electron interactions, Phys. Rev. B **104**, 035433 (2021).

[42] T. B. Boykin, G. Klimeck, and F. Oyafuso, Valence band effective-mass expressions in the $sp^3d^5s^*$ empirical tight-binding model applied to a Si and Ge parametrization, Phys. Rev. B **69**, 115201 (2004).

[43] G. P. Lansbergen, R. Rahman, C. J. Wellard, I. Woo, J. Caro, N. Collaert, S. Biesemans, G. Klimeck, L. C. L. Hollenberg, and S. Rogge, Gate-induced quantum-confinement transition of a single dopant atom in a silicon FinFET, Nat. Phys. **4**, 656 (2008).

[44] J. Salfi, J. Mol, R. Rahman, G. Klimeck, M. Simmons, L. Hollenberg, and S. Rogge, Spatially resolving valley quantum interference of a donor in silicon, Nat. Mater. **13**, 605 (2014).

[45] R. Rahman, C. J. Wellard, F. R. Bradbury, M. Prada, J. H. Cole, G. Klimeck, and L. C. L. Hollenberg, High Precision Quantum Control of Single Donor Spins in Silicon, Phys. Rev. Lett. **99**, 036403 (2007).

[46] R. Rahman, S. H. Park, T. B. Boykin, G. Klimeck, S. Rogge, and L. C. L. Hollenberg, Gate-induced g-factor control and dimensional transition for donors in multivalley semiconductors, Phys. Rev. B **80**, 155301 (2009).

[47] Y.-L. Hsueh, H. Büch, Y. Tan, Y. Wang, L. C. L. Hollenberg, G. Klimeck, M. Y. Simmons, and R. Rahman, Spin-Lattice Relaxation Times of Single Donors and Donor Clusters in Silicon, Phys. Rev. Lett. **113**, 246406 (2014).

[48] G. Klimeck, S. S. Ahmed, H. Bae, N. Kharche, S. Clark, B. Haley, S. Lee, M. Naumov, H. Ryu, F. Saied, M. Prada, M. Korkusinski, T. B. Boykin, and R. Rahman, Atomistic simulation of realistically sized nanodevices using NEMO 3-D–Part I: Models and benchmarks, IEEE Trans. Electron Devices **54**, 2079 (2007).

[49] R. Rahman, G. P. Lansbergen, J. Verduijn, G. C. Tettamanzi, S. H. Park, N. Collaert, S. Biesemans, G. Klimeck, L. C. L. Hollenberg, and S. Rogge, Electric field reduced charging energies and two-electron bound excited states of single donors in silicon, Phys. Rev. B **84**, 115428 (2011).

[50] Y. Wang, A. Tankasala, L. C. L. Hollenberg, G. Klimeck, M. Y. Simmons, and R. Rahman, Highly tunable exchange in donor qubits in silicon, npj Quantum Inf. **2**, 16008 (2016).

[51] J. A. Mol, J. Salfi, R. Rahman, Y. Hsueh, J. A. Miwa, G. Klimeck, M. Y. Simmons, and S. Rogge, Interface-induced heavy-hole/light-hole splitting of acceptors in silicon, Appl. Phys. Lett. **106**, 203110 (2015).